A generalized Gaussian overlap model for fluids of anisotropic particles

Gary Ayton and G. N. Patey

Citation: The Journal of Chemical Physics **102**, 9040 (1995); doi: 10.1063/1.468852
View online: http://dx.doi.org/10.1063/1.468852
View Table of Contents: http://scitation.aip.org/content/aip/journal/jcp/102/22?ver=pdfcov
Published by the AIP Publishing

A generalized Gaussian overlap model for fluids of anisotropic particles

Gary Ayton and G. N. Patey
Department of Chemistry, University of British Columbia, Vancouver, British Columbia, Canada V6T 1Z1

(Received 4 January 1995; accepted 22 February 1995)

The Gaussian overlap model for anisotropic particles is generalized to include ellipsoids which are not axially symmetric. Explicit analytical expressions are given for the potential and for the torques necessary in molecular dynamics (MD) simulations. Employing this model, we have obtained MD results for several systems carefully selected to determine the influence of molecular biaxiality upon the formation of uniaxial nematic phases. By comparing systems of biaxial and axially symmetric particles with the same length-to-breadth ratio and at the same reduced density and temperature, it is clearly shown that even relatively little molecular ''flatness'' can significantly favor the formation of a uniaxial nematic phase. For example, ellipsoids characterized by the aspect ratios 2:3:9 form a stable nematic whereas the axially symmetric counterpart (i.e., 3:3:9) has no stable liquid crystal phase. © *1995 American Institute of Physics.*

I. INTRODUCTION

Theoretical studies and computer simulations of liquid crystals require a pair potential that captures the anisotropy of interactions in real systems. Of course, molecular shape can be modeled at various degrees of complexity. If one wishes to model a specific system in detail, then employing a site–site interaction model[1] is perhaps the best alternative. However, this is computationally very expensive, particularly for molecules sufficiently large to form liquid crystals. A simple more general approach is to employ a shape which represents a class of particles. For example, axially symmetric hard models such as spherocylinders,[2] cut spheres,[3] and ellipsoids[4] have received considerable attention.[5] Much less effort has been focused upon the simulation of hard particles which lack axial symmetry. An important exception is the Monte Carlo study of Allen[6] which showed that for some anisotropies a biaxial nematic phase exists and lies between uniaxial nematic and uniaxial nematic discotic phases.

Another approach to shape-dependent intermolecular potentials is the Gaussian overlap model suggested by Berne and Pechukas.[7] This method gives continuous interaction potentials which are very convenient for molecular dynamics (MD) simulations. Also, extensions of this method are used to construct the so-called Gay–Berne potentials[8] which have been employed in recent simulations of liquid crystals.[9–12] However, to date this approach has been limited to systems of axially symmetric particles. In the present paper we describe a generalized Gaussian overlap model where the constraint of axial symmetry has been removed.

In the spirit of the original Berne–Pechukas model, molecular shape is approximated by a three-dimensional Gaussian of general ellipsoidal symmetry. It is then assumed that the repulsive pair interaction of two molecules is proportional to the overlap volume of the Gaussians. This yields an interaction potential which depends upon the orientation and separation of the two Gaussians. The new form derived here applies to ellipsoids with nondegenerate semiaxes. The potential decays as a scaled Gaussian and the maximum height can be varied while holding the width constant; in the limit that the height becomes infinite the ellipsoids become ''hard.'' Of course, as with the original Berne–Pechukas model, the present interaction is physically unrealistic in that one would expect algebraic rather than Gaussian decay. However, repulsive interactions are very short ranged and we would not expect the exact nature of the decay to be of crucial importance. Obviously, this is the same assumption underlying the widespread use of hard core models. The strength of the Gaussian overlap model lies in its ability to represent molecular shape and in its computational convenience. The calculation of the forces and torques necessary in MD simulations is greatly simplified by the Gaussian form. In addition to deriving the generalized Gaussian overlap repulsive interaction, we suggest a simple related expression which might be used to model short-range attractive interactions.

As a physically interesting application of the generalized Gaussian overlap model, we have investigated the influence of molecular biaxiality on the formation of uniaxial nematic phases. In addition to having relatively large length-to-breadth ratios (discotics are not included in this discussion), the molecules of real liquid crystals tend to be somewhat flat due to the presence of rigid aromatic rings.[13] However, in model calculations the uniaxial ordering is usually presumed to arise from particle elongation and the role of flatness has received scant attention. For example, it would be interesting to know if, and to what extent, introducing particle flatness can create uniaxial nematic order in systems where the particle elongation alone is insufficient to do so. We note that this question was not addressed in Allen's earlier simulations[6] which focused upon locating biaxial transitions in model systems already possessing uniaxial order. Here we report the results of a series of MD simulations carefully designed to determine the influence of molecular flatness. We begin with a system of axially symmetric particles which has no liquid crystal phase whatsoever and then slowly flatten the particles keeping all other variables (i.e., the reduced density, reduced temperature, and the remaining two aspect ratios) fixed. As the particles become flatter we observe a transition from an isotropic to a uniaxial nematic phase. This transition results entirely from increasing particle flatness and clearly demonstrates that molecular biaxiality can be an

 0021-9606/95/102(22)/9040/8/$6.00

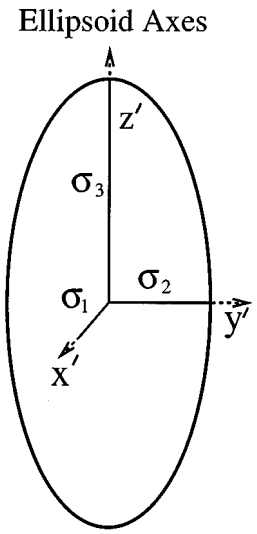

FIG. 1. A sketch showing the molecular axes (x',y',z') and the principal radii σ_1, σ_2, and σ_3 which characterize the ellipsoid model.

important factor in the formation of uniaxial phases. As the particles are made flatter still a uniaxial to biaxial transition is also observed.

II. GENERALIZED GAUSSIAN OVERLAP INTEGRAL

A three-dimensional Gaussian function centered at the point $\mathbf{p}$ with orientation (θ,ϕ,ψ) can be defined as

$$j(\mathbf{r}) = \gamma\, e^{s/2 - s\mathbf{T}:(\mathbf{r}-\mathbf{p})(\mathbf{r}-\mathbf{p})}. \tag{2.1}$$

The parameter s determines the maximum of the Gaussian when $\mathbf{r}=\mathbf{p}$. When $\mathbf{r}$ lies on the surface of the ellipsoid defined by

$$2\mathbf{T}:(\mathbf{r}-\mathbf{p})(\mathbf{r}-\mathbf{p}) = 1, \tag{2.2}$$

then

$$j(\mathbf{r}) = \gamma. \tag{2.3}$$

The value of γ will be chosen after the overlap integral is calculated. The orientation and shape of the Gaussian in the space fixed frame are given by the second rank tensor $\mathbf{T}$. It is defined by

$$\mathbf{T} = \mathbf{R}^t\mathbf{b}\mathbf{R}, \tag{2.4a}$$

where $\mathbf{b}$ is the tensor

$$\begin{pmatrix} 1/2\sigma_1^2 & 0 & 0 \\ 0 & 1/2\sigma_2^2 & 0 \\ 0 & 0 & 1/2\sigma_3^2 \end{pmatrix}. \tag{2.4b}$$

The parameters σ_1, σ_2, and σ_3 are the principle radii when the ellipsoid is cast in standard form (see Fig. 1). $\mathbf{R}$ is a rotation matrix (its transpose is denoted $\mathbf{R}^t$) which expressed in quaternions has the form[14]

$$\begin{pmatrix} q_0^2+q_1^2-q_2^2-q_3^2 & 2(q_1q_2+q_0q_3) & 2(q_1q_3-q_0q_2) \\ 2(q_1q_2-q_0q_3) & q_0^2-q_1^2+q_2^2-q_3^2 & 2(q_2q_3+q_0q_1) \\ 2(q_1q_3+q_0q_2) & 2(q_2q_3-q_0q_1) & q_0^2-q_1^2-q_2^2+q_3^2 \end{pmatrix}, \tag{2.4c}$$

where

$$q_0 = \cos\tfrac{1}{2}\theta\, \cos\tfrac{1}{2}(\phi+\psi), \tag{2.4d}$$

$$q_1 = \sin\tfrac{1}{2}\theta\, \cos\tfrac{1}{2}(\phi-\psi), \tag{2.4e}$$

$$q_2 = \sin\tfrac{1}{2}\theta\, \sin\tfrac{1}{2}(\phi-\psi), \tag{2.4f}$$

$$q_3 = \cos\tfrac{1}{2}\theta\, \sin\tfrac{1}{2}(\phi+\psi). \tag{2.4g}$$

The choice of quaternions to express orientations simplifies the computations. The calculation of trigonometric functions is avoided in the rotation matrix, and the equations of motion have no discontinuities.[14]

We next consider the overlap integral of two Gaussians, i and j, where i is centered at the origin and j at $\mathbf{p}$. The overlap integral can be written as

$$I(\mathbf{p},\mathbf{q}_i,\mathbf{q}_j) = \gamma^2\, e^s \int_{-\infty}^{\infty}\int_{-\infty}^{\infty}\int_{-\infty}^{\infty} e^{-s[\mathbf{T}_i:\mathbf{rr}+\mathbf{T}_j:(\mathbf{r}-\mathbf{p})(\mathbf{r}-\mathbf{p})]} \times dr_z\, dr_y\, dr_x, \tag{2.5}$$

and some details of the integration are given in Appendix A. The result obtained can be expressed in the compact form

$$I(\mathbf{p},\mathbf{q}_i,\mathbf{q}_j) = \frac{\gamma^2}{\sqrt{|\mathbf{T}_i+\mathbf{T}_j|}}\left(\frac{\pi}{s}\right)^{3/2} e^{s[1+(\mathbf{BB}/4A-\mathbf{C}):\mathbf{pp}]}, \tag{2.6}$$

where the scalar $A \equiv a''/s$ and the elements of the vector $\mathbf{B}$ and of the tensor $\mathbf{C}$ are given explicitly in Appendix A.

In order to associate Eq. (2.6) with a repulsive pair potential, γ^2 must have the units of energy per unit volume. If we consider identical ellipsoids and choose

$$\gamma = 2\sqrt{2\epsilon}\left(\frac{s}{\pi}\right)^{3/4}(2|\mathbf{b}|)^{1/4}, \tag{2.7}$$

then the interaction energy $V(\mathbf{p},\mathbf{q}_i,\mathbf{q}_j)$ is given by

$$V(\mathbf{p},\mathbf{q}_i,\mathbf{q}_j) = \frac{4\epsilon\sqrt{|\mathbf{b}_i+\mathbf{b}_j|}}{\sqrt{|\mathbf{T}_i+\mathbf{T}_j|}}\, e^{s[1+(\mathbf{BB}/4A-\mathbf{C}):\mathbf{pp}]}. \tag{2.8}$$

For this particular choice of γ the energy is $4\epsilon e^s$ when the ellipsoids are aligned and the intermolecular distance is zero. This is true regardless of the size or aspect ratios of the ellipsoids. The factor of 4 will scale the well depth when the attractive term is added.

Equation (2.8) is a purely repulsive potential which can be used to model the hard core or ''shape'' of a molecule. However, it is possible to add simple attractive terms without loss of generality or the introduction of computational difficulties. For example, we may choose the attractive term

$$V_{\mathrm{att}}(\mathbf{p},\mathbf{q}_i,\mathbf{q}_j) = -\frac{4\epsilon\sqrt{|\mathbf{b}_i+\mathbf{b}_j|}}{\sqrt{|\mathbf{T}_i+\mathbf{T}_j|}}\, e^{s/2[1+(\mathbf{BB}/4A-\mathbf{C}):\mathbf{pp}]}, \tag{2.9}$$

such that the total pair potential is given by

$$V(\mathbf{p},\mathbf{q}_i,\mathbf{q}_j)=\frac{4\epsilon\sqrt{|\mathbf{b}_i+\mathbf{b}_j|}}{\sqrt{|\mathbf{T}_i+\mathbf{T}_j|}}\,(e^{s[1+(\mathbf{BB}/4A-\mathbf{C}):\mathbf{pp}]} - e^{s/2[1+(\mathbf{BB}/4A-\mathbf{C}):\mathbf{pp}]}). \tag{2.10}$$

This attractive term is simply a negative Gaussian with a maximum of $e^{s/2}$. The factor of 4 scales the well depth so that the minimum for two spherical Gaussians is $-\epsilon$, independent of the scale factor, and comparable with the well depth of a Lennard-Jones potential. Of course, this attractive potential has a Gaussian decay and will not reproduce the correct long-range behavior of the dispersion interactions. Nevertheless, it is computationally very convenient and it should capture many of the more robust features of short-range attractive interactions.

The repulsive potential given in Eq. (2.8) is continuous and it is possible to obtain analytical expressions for the forces and torques. This involves taking the gradient of the pair potential with respect to the intermolecular vector **p** and with respect to the eight quaternion parameters which define the orientation of the two ellipsoids. The procedure is given in Appendix B.

III. RESULTS

If we take σ as our fundamental unit of length and ϵ as our fundamental unit of energy, then a system of Gaussian ellipsoids can be characterized by the reduced density $\rho^*=8N\sigma_1\sigma_2\sigma_3/V$ (N is the number of particles and V is the volume) and the reduced temperature $T^*=k_BT/\epsilon$ (k_BT is the Boltzmann constant times the absolute temperature). It is also useful to introduce the reduced energy $U^*=U/\epsilon$, the reduced pressure $P^*=P\sigma^3/\epsilon$, and the reduced time $t^*=\sqrt{\epsilon/\sigma^2 m}$, where m is the mass of a particle. Henceforth, it should be understood that all lengths are quoted in units of σ and all energies in units of ϵ.

Suitable moments of inertia about the molecular axis (x',y',z') (see Fig. 1), $I_{\alpha'\alpha'}$, can be calculated by assuming a mass density of the form $\zeta\, e^{s/2-s\mathbf{b}:\mathbf{rr}}$, where ζ is a constant and has units of mass per unit volume. One obtains

$$I_{x'x'}=\alpha(\sigma_2^2+\sigma_3^2), \tag{3.1a}$$

$$I_{y'y'}=\alpha(\sigma_1^2+\sigma_3^2), \tag{3.1b}$$

$$I_{z'z'}=\alpha(\sigma_1^2+\sigma_2^2), \tag{3.1c}$$

where $\alpha=\zeta\, e^{s/2}\sigma_1\sigma_2\sigma_3(\pi/s)^{3/2}$. In MD simulations it is advantageous to have similar relaxation rates for translations and reorientations. That is, the decay of velocity–velocity and angular-velocity–angular-velocity autocorrelation functions should be similar.[14] This can be accomplished by adjusting ζ. Also, as usual, it is convenient to define reduced moments of inertia of the form $I^*_{\alpha'\alpha'}=I_{\alpha'\alpha'}/m\sigma^2$.

In MD simulations, the existence of liquid crystal phases is established by monitoring both dynamic and static observables. The mean square displacement $\langle|\mathbf{r}(t)-\mathbf{r}(0)|^2\rangle$ was used as a diagnostic to determine if a particular system was liquid or solid. For all systems studied, the mean square displacement increased with time indicating fluid behavior. Uniaxial and biaxial ordering was detected by calculating the second rank order parameters Q^2_{00} and Q^2_{22}, defined as[6,15]

$$Q^2_{00}=\langle\tfrac{1}{2}(3\cos^2\theta-1)\rangle, \tag{3.2a}$$

$$Q^2_{22}=\langle\tfrac{1}{2}(1+\cos^2\theta)\cos 2\phi\,\cos 2\psi - \cos\theta\,\sin 2\phi\,\sin 2\psi\rangle, \tag{3.2b}$$

where the Euler angles describing molecular orientation are now defined with respect to the laboratory fixed reference frame (X,Y,Z) selected as described below. Q^2_{00} is the usual uniaxial order parameter and (except for finite size effects) will be zero in the isotropic phase. Q^2_{22} is a biaxial order parameter which will be zero in isotropic and uniaxial phases but nonzero in a biaxial phase.

Following Allen,[6] we calculate the order parameters by first forming the ordering matrices $\mathbf{Q}^{xx}$, $\mathbf{Q}^{yy}$, and $\mathbf{Q}^{zz}$ with elements defined by

$$Q^{xx}_{\alpha\beta}=\frac{1}{N}\sum_{i=1}^{N}\frac{1}{2}(3\hat{x}_{i_\alpha}\hat{x}_{i_\beta}-\delta_{\alpha\beta}),\quad \alpha,\beta=1,2,3 \tag{3.3}$$

(and similar expressions for $Q^{yy}_{\alpha\beta}$ and $Q^{zz}_{\alpha\beta}$), where $\hat{\mathbf{x}}_i$, $\hat{\mathbf{y}}_i$, and $\hat{\mathbf{z}}_i$ are unit vectors along the three symmetry axes of particle i. We next determine the largest eigenvalue associated with each of the three matrices. The molecular axis corresponding to the largest of these three is identified as the principal molecular z axis and the corresponding eigenvector becomes the laboratory fixed Z axis. The second largest and smallest eigenvalues are used to identify the molecular y and x axes, respectively. The associated eigenvectors are then orthogonalized together with Z in order to construct the Y and X axis of the laboratory fixed frame. In terms of these axes, the order parameters have the Cartesian form

$$Q^2_{00}=\langle\mathbf{Z}\cdot\mathbf{Q}^{zz}\cdot\mathbf{Z}\rangle, \tag{3.4a}$$

$$Q^2_{22}=\tfrac{1}{3}\langle\mathbf{X}\cdot\mathbf{Q}^{xx}\cdot\mathbf{X}+\mathbf{Y}\cdot\mathbf{Q}^{yy}\cdot\mathbf{Y}-\mathbf{X}\cdot\mathbf{Q}^{yy}\cdot\mathbf{X}-\mathbf{Y}\cdot\mathbf{Q}^{xx}\cdot\mathbf{Y}\rangle. \tag{3.4b}$$

These averages can be easily evaluated in the simulation. It is important to note that the variable molecular x, y, and z

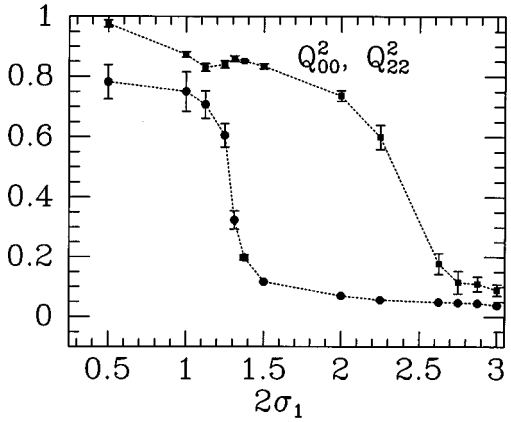

FIG. 2. Order parameters as a function of particle thickness at fixed reduced temperature and density. The squares are the uniaxial order parameter Q^2_{00} and the circles are the biaxial order parameter Q^2_{22}. The error bars represent one standard deviation.

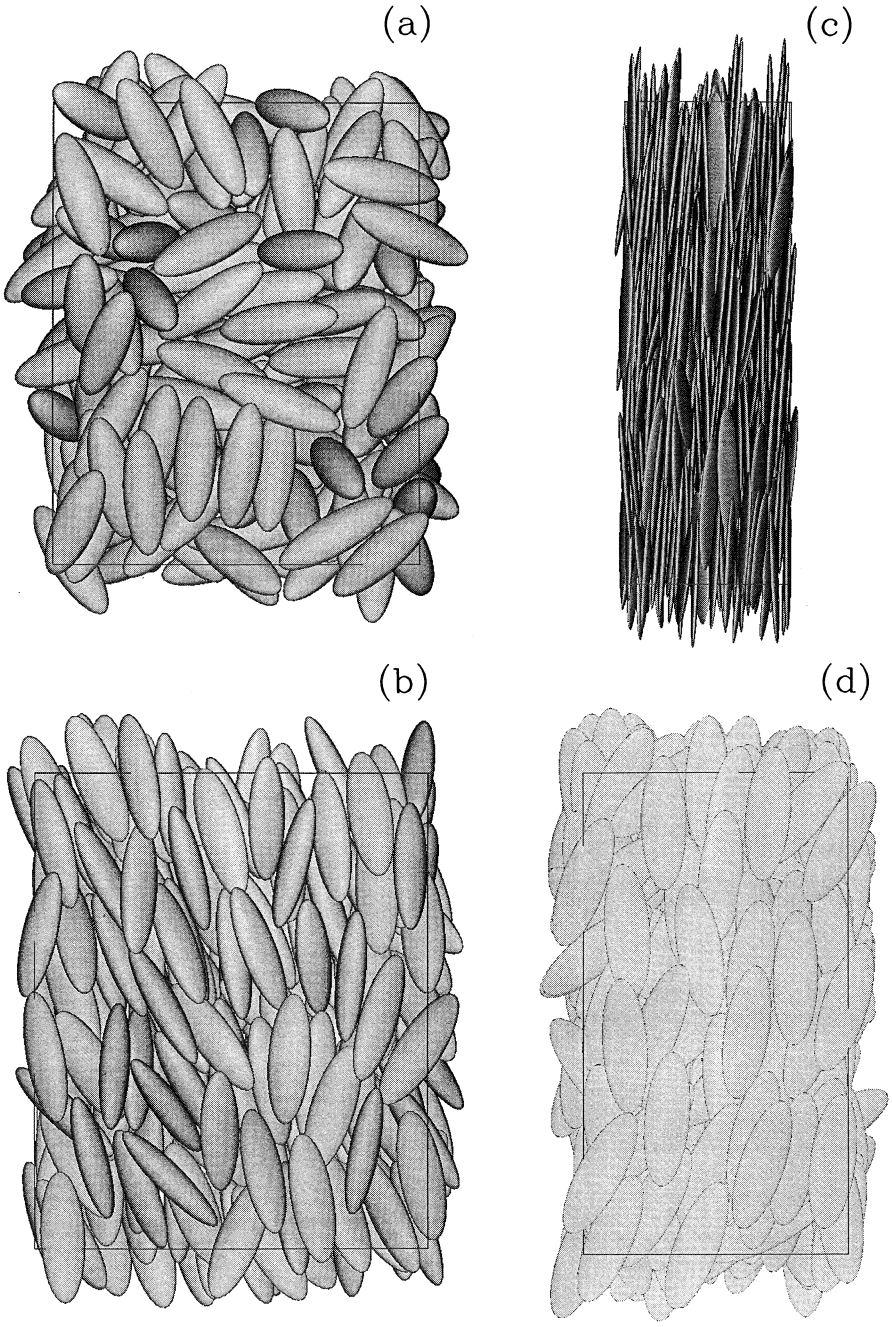

FIG. 3. Snapshots of instantaneous configurations for: (a) an isotropic phase with $2\sigma_1:2\sigma_2:2\sigma_3=2.875:3:9$; (b) a uniaxial phase with $2\sigma_1:2\sigma_2:2\sigma_3=2.25:3:9$; (c), (d) a biaxial phase with $2\sigma_1:2\sigma_2:2\sigma_3=0.875:3:9$. In (b) the director is along the z' axis (up and down on the page). In (c) and (d) the directors are along x' and z'. The snapshots are taken along the axes perpendicular to the z' director.

axes referred to in this paragraph are used only in the definition of the order parameters. They should not be confused with the fixed molecular coordinate system (x',y',z') shown in Fig. 1.

We have investigated the effects of molecular flatness on liquid crystal phase transitions by carrying out MD simulations of selected repulsive Gaussian ellipsoids. The simulations were performed using quaternion coordinates as described in Refs. 14 and 16. The length $2\sigma_1$ was varied from 0.5 to 3 while the remaining dimensions were held fixed. The σ_2 and σ_3 radii were chosen such that the ellipsoid of revolution obtained when $\sigma_1=\sigma_2$ has $2\sigma_1:2\sigma_2:2\sigma_3\equiv3:3:9$. These dimensions were selected because prolate hard ellipsoids of revolution with an aspect ratio of 1:3 are believed to have no stable liquid crystal phase.[17] Thus, at fixed temperature and reduced density, any ordering found by varying σ_1 can be attributed to molecular flatness. All results reported are for the reduced parameters $T^*=1.35$ and $\rho^*=0.8$. The scale parameter s was set at 20 which gives a very hard potential. Some runs were also carried out with s values of 10 and 100 and similar phase behavior was observed. We note that for hard ellipsoids with principal radii σ_1, σ_2, and σ_3, the value

TABLE I. Reduced energies and pressures for selected systems.

$2\sigma_1$:$2\sigma_2$:$2\sigma_3$	$\langle U^* \rangle / N$	$\langle P^* \rangle / N$
0.5:3:9	1.314±0.008	1.178±0.01
1:3:9	1.325±0.008	0.592±0.01
2:3:9	1.287±0.010	0.288±0.005
3:3:9	1.336±0.016	0.199±0.002

of ρ^* used would correspond to $\rho/\rho_{cp}=0.8/\sqrt{2}=0.5657$, where ρ_{cp} is the close packing density.

Most calculations were carried out with 216 particles in a noncubic simulation cell starting from a body-centered orthorhombic lattice. For systems with $2\sigma_1$:$2\sigma_2$:$2\sigma_3$ ranging from 1:3:9 to 2:3:9, the initial particle array was $12\times6\times3$. For systems with $2\sigma_1>2$, the initial particle array was $6\times12\times3$. Systems with $2\sigma_1<1$ were done with 360 particles to ensure that the simulation cell did not become too narrow in one direction. Possible system size and/or cell shape dependence was examined by carrying out simulations of several systems using 216, 288, and 360 particles. The results obtained were found to be very similar and there was no significant dependence upon system size. In all simulations, the reduced time step $\delta t^*=0.0012$ was used and the moment of inertia parameter ζ was adjusted to keep $\alpha=0.5$. Typically, systems were equilibrated for 100 000 time steps and this was followed by ''production runs'' of 100 000 time steps. Standard deviations were estimated by dividing the production runs into ten equal blocks and assuming that the block averages were independent measurements.

In Fig. 2, the order parameters Q_{00}^2 and Q_{22}^2 are plotted as a function of the particle thickness $2\sigma_1$. We emphasize again that for the points shown in this plot, the lengths $2\sigma_2$ and $2\sigma_3$ are held fixed (at 3 and 9, respectively) as are the reduced temperature and density. Thus Fig. 2 displays only the influence of changing width; as $2\sigma_1$ is varied from 3 to 0.5 we go from axially symmetric ellipsoids of revolution to flat, surfboard-like particles. Snapshots of various systems are shown in Fig. 3 and these give a clear physical picture of the particles involved.

We see from Fig. 2 that, as expected, when the aspect ratios are close to 3:3:9 the liquids are isotropic [see Fig. 3(a)] and apart from small finite size effects both order parameters are zero. However, as $2\sigma_1$ is reduced the system quickly orders to form a uniaxial nematic phase [see Fig. 3(b)] with the z' molecular axes (see Fig. 1) aligned along the director. This clearly shows that *molecular biaxiality* can have a very strong effect even upon the formation of a *uniaxial* phase. It is evident that as the particles become flatter the tendency to form a liquid crystal phase is significantly increased. At $2\sigma_1\approx1.2$, Q_{22}^2 increases sharply indicating the formation of a biaxial phase [see Figs. 3(c) and 3(d)]. Also, at $2\sigma_1\approx1.1$, Q_{00}^2 increases rather sharply as well indicating that the principal uniaxial director is now associated with the x' rather than then the z' axes of the molecules. With respect to Fig. 2, it should be noted that Q_{22}^2 does not approach 1 as $2\sigma_1$ is decreased. This is because as the particles become thinner the ordering of the z' molecular axes is diminished and, eventually, for $2\sigma_1$ sufficiently small, we would expect to obtain a uniaxial discotic phase.

Some examples of the average reduced energies and pressures obtained per particle are given in Table I. The actual values of the energy and pressure do not have much physical significance in the present context but it is useful to include some numbers for comparison if others are to use this model in future work. We do note that the energies obtained are small and positive and do not vary significantly with changing aspect ratios. The pressure does increase systematically as the particles become flatter.

IV. CONCLUSIONS

In this paper we have generalized the Gaussian overlap model to include ellipsoidal particles of nonaxial symmetry. The continuous, repulsive, pair potential obtained is particularly convenient for MD simulations because the necessary forces and torques can be readily obtained. Explicit analytical expressions for the torques have been included. We have also suggested a simple method of including attractive forces which may prove useful for some systems.

Our principal motivation in developing the generalized Gaussian overlap potential was the need to include molecular shape more realistically in model liquid crystals. More precisely, we wished to examine the influence of molecular flatness upon liquid crystal phase transitions. Towards this end, we have carried out systematic, constant temperature MD simulations keeping two principal radii fixed. Then, by varying the remaining radius while holding the reduced density constant, we were able to clearly show the important influence of molecular flatness on the formation of nematic liquid crystals. It was demonstrated that even a little molecular biaxiality can strongly favor the formation of a uniaxial nematic phase. That is, flatness in one direction can help stabilize ordering in another. For example, at a reduced density where particles characterized by the aspect ratios 3:3:9 are isotropic, those with ratios 2:3:9 form a strongly ordered uniaxial nematic phase. As the particles become flatter the expected biaxial nematic phase is obtained. For the present model, particles with the aspect ratios 1:3:9 formed a fully developed biaxial phase.

It would be interesting to further elucidate the phase behavior of the generalized Gaussian model and work in that direction is underway. We also plan to examine the dynamical properties of the uniaxial and biaxial nematic phases.

ACKNOWLEDGMENT

The financial support of the Natural Sciences and Engineering Research Council of Canada is gratefully acknowledged.

APPENDIX A: EVALUATION OF THE OVERLAP INTEGRAL

The overlap integral of two three-dimensional Gaussians can be written as

$$I(\mathbf{p},\mathbf{q}_i,\mathbf{q}_j)=\gamma^2\ e^s\int_{-\infty}^{\infty}\int_{-\infty}^{\infty}\int_{-\infty}^{\infty} e^{-s[\mathbf{T}_i:\mathbf{rr}+\mathbf{T}_j:(\mathbf{r}-\mathbf{p})(\mathbf{r}-\mathbf{p})]} \times dr_z\ dr_y\ dr_x, \tag{A1}$$

and evaluated by application of standard integrals. However, it is useful to give some intermediate results which are required in the expressions for the torques obtained in Appendix B.

Integration with respect to r_z yields

$$\int_{-\infty}^{\infty} e^{-(ar_z^2+br_z+c)}\ dr_z=\frac{\pi^{1/2}}{\sqrt{a}}\ e^{b^2/4a-c}, \tag{A2a}$$

where

$$\frac{a}{s}=T_{i_{zz}}+T_{j_{zz}}, \tag{A2b}$$

$$\frac{b}{s}=2[T_{i_{xz}}r_x+T_{j_{xz}}(r_x-p_x)+T_{i_{yz}}r_y+T_{j_{yz}}(r_y-p_y) -T_{j_{zz}}p_z], \tag{A2c}$$

$$\frac{c}{s}=T_{j_{zz}}p_{zz}^2-2[T_{j_{xz}}(r_x-p_x)+T_{j_{yz}}(r_y-p_y)]p_z. \tag{A2d}$$

Collecting terms in descending powers of r_y yields

$$\frac{\pi^{1/2}}{\sqrt{a}}\int_{-\infty}^{\infty} e^{-(a'r_y^2+b'r_y+c')}\ dr_y=\frac{\pi}{\sqrt{aa'}}\ e^{b'^2/4a'-c'}, \tag{A3a}$$

where

$$\frac{a'}{s}=\frac{S_{yy}S_{zz}-S_{yz}^2}{S_{zz}}, \tag{A3b}$$

$$\frac{b'}{s}=\frac{b'_{(r_x)}}{s}\ r_x+\frac{b'_{(1)}}{s}, \tag{A3c}$$

$$\frac{b'_{(r_x)}}{s}=2\left(S_{xy}-\frac{S_{yz}S_{xz}}{S_{zz}}\right), \tag{A3d}$$

$$\frac{b'_{(1)}}{s}=2\left[\frac{S_{yz}}{S_{zz}}\ (T_{j_{xz}}p_x+T_{j_{yz}}p_y+T_{j_{zz}}p_z) -(T_{j_{xy}}p_x+T_{j_{yy}}p_y+T_{j_{zy}}p_z)\right], \tag{A3e}$$

$$\frac{c'}{s}=T_{j_{yy}}p_y^2-2T_{j_{xy}}(r_x-p_x)p_y-\frac{1}{S_{zz}}[T_{i_{xz}}r_x+T_{j_{xz}}(r_x -p_x)-T_{j_{yz}}p_y-T_{j_{zz}}p_z]^2 -2[T_{j_{xz}}(r_x-p_x)-T_{j_{yz}}p_y]p_z+T_{j_{zz}}p_z^2, \tag{A3f}$$

and the tensor $\mathbf{S}$ is defined by

$$\mathbf{S}=\mathbf{T}_i+\mathbf{T}_j. \tag{A3g}$$

Finally, terms are collected in descending powers of r_x to obtain

$$\frac{\pi}{\sqrt{aa'}}\int_{-\infty}^{\infty} e^{-(a''r_x^2+b''r_x+c'')}\ dr_x=\frac{\pi^{3/2}}{\sqrt{aa'a''}}\ e^{b''^2/4a''-c''}, \tag{A4a}$$

where

$$\frac{a''}{s}=\frac{|\mathbf{T}_i+\mathbf{T}_j|}{S_{yy}S_{zz}-S_{yz}^2}, \tag{A4b}$$

$$\frac{b''}{s}=\mathbf{B}\cdot\mathbf{p}, \tag{A4c}$$

$$\frac{c''}{s}=\mathbf{C}:\mathbf{pp}. \tag{A4d}$$

The components of the vector $\mathbf{B}$ are

$$B_x=\frac{-2}{S_{yy}S_{zz}-S_{yz}^2}\begin{vmatrix} T_{j_{xx}} & T_{j_{xy}} & T_{j_{xz}} \\ S_{yx} & S_{yy} & S_{yz} \\ S_{zx} & S_{zy} & S_{zz}\end{vmatrix}, \tag{A5a}$$

$$B_y=\frac{-2}{S_{yy}S_{zz}-S_{yz}^2}\begin{vmatrix} T_{j_{xy}} & T_{j_{yy}} & T_{j_{zy}} \\ S_{yx} & S_{yy} & S_{yz} \\ S_{zx} & S_{zy} & S_{zz}\end{vmatrix}, \tag{A5b}$$

$$B_z=\frac{-2}{S_{yy}S_{zz}-S_{yz}^2}\begin{vmatrix} T_{j_{xz}} & T_{j_{yz}} & T_{j_{zz}} \\ S_{yx} & S_{yy} & S_{yz} \\ S_{zx} & S_{zy} & S_{zz}\end{vmatrix}. \tag{A5c}$$

The elements of the symmetric tensor $\mathbf{C}$ are

$$C_{xx}=T_{j_{xx}}-\frac{(S_{yz}T_{j_{xz}}-S_{zz}T_{j_{xy}})^2}{S_{zz}(S_{yy}S_{zz}-S_{yz}^2)}-\frac{T_{j_{xz}}^2}{S_{zz}}, \tag{A6a}$$

$$C_{yy}=T_{j_{yy}}-\frac{(S_{yz}T_{j_{yz}}-S_{zz}T_{j_{yy}})^2}{S_{zz}(S_{yy}S_{zz}-S_{yz}^2)}-\frac{T_{j_{yz}}^2}{S_{zz}}, \tag{A6b}$$

$$C_{zz}=T_{j_{zz}}-\frac{(S_{yz}T_{j_{zz}}-S_{zz}T_{j_{zy}})^2}{S_{zz}(S_{yy}S_{zz}-S_{yz}^2)}-\frac{T_{j_{zz}}^2}{S_{zz}}, \tag{A6c}$$

$$C_{xy}=T_{j_{xy}}-\frac{(S_{yz}T_{j_{xz}}-S_{zz}T_{j_{xy}})(S_{yz}T_{j_{yz}}-S_{zz}T_{j_{yy}})}{S_{zz}(S_{yy}S_{zz}-S_{yz}^2)} -\frac{T_{j_{xz}}T_{j_{yz}}}{S_{zz}}, \tag{A6d}$$

$$C_{xz}=T_{j_{xz}}-\frac{(S_{yz}T_{j_{xz}}-S_{zz}T_{j_{xy}})(S_{yz}T_{j_{zz}}-S_{zz}T_{j_{zy}})}{S_{zz}(S_{yy}S_{zz}-S_{yz}^2)} -\frac{T_{j_{xz}}T_{j_{zz}}}{S_{zz}}, \tag{A6e}$$

$$C_{yz}=T_{j_{yz}}-\frac{(S_{yz}T_{j_{yz}}-S_{zz}T_{j_{yy}})(S_{yz}T_{j_{zz}}-S_{zz}T_{j_{zy}})}{S_{zz}(S_{yy}S_{zz}-S_{yz}^2)} -\frac{T_{j_{yz}}T_{j_{zz}}}{S_{zz}}. \tag{A6f}$$

APPENDIX B: FORCES AND TORQUES

Here we give expressions for the forces and torques needed in MD simulations. If a continuous potential is employed, the forces and torques can be found by taking the appropriate gradients of the potential. For the present model the force on particle i due to j is easily obtained using

$$f_{ij} = -\boldsymbol{\nabla}_{\mathbf{p}_{ij}} V_{ij} \tag{B1a}$$

and

$$f_{ji} = -f_{ij}. \tag{B1b}$$

The torque on particle i (at the origin) due to j (at $\mathbf{p}$), $\boldsymbol{\tau}_{ij}^{b}$ (defined in the body-fixed frame of particle i) is given by[16]

$$\boldsymbol{\tau}_{ij}^{b} = -\tfrac{1}{2}\tilde{\mathbf{Q}}_i \boldsymbol{\nabla}_{\mathbf{Q}_i} V_{ij}, \tag{B2a}$$

where

$$\tilde{\mathbf{Q}}_i = [q_{i_0}, -(q_{i_1}\hat{i} + q_{i_2}\hat{j} + q_{i_3}\hat{k})], \tag{B2b}$$

and we have defined the operator

$$\boldsymbol{\nabla}_{\mathbf{Q}_i} = \left(\frac{\partial}{\partial q_{i_0}}, \frac{\partial}{\partial q_{i_1}}\hat{i} + \frac{\partial}{\partial q_{i_2}}\hat{j} + \frac{\partial}{\partial q_{i_3}}\hat{k} \right). \tag{B2c}$$

The calculation of $\boldsymbol{\tau}_{ij}^{b}$ requires the evaluation of partial derivatives of the form

$$\frac{\partial V_{ij}}{\partial q_{i_k}} = \gamma^2 e^s \int_{-\infty}^{\infty}\int_{-\infty}^{\infty}\int_{-\infty}^{\infty} s\mathbf{T}'_{i_k} : \mathbf{rr}\, e^{-s[\mathbf{T}_i : \mathbf{rr} + \mathbf{T}_j : (\mathbf{r}-\mathbf{p})(\mathbf{r}-\mathbf{p})]} \times dr_z\, dr_y\, dr_x, \tag{B3a}$$

where $k = 0,1,2,3$ and the elements of $\mathbf{T}'_{i_k}$ are

$$T'_{i_{k\alpha\beta}} = \frac{\partial T_{i_{\alpha\beta}}}{\partial q_{i_k}}. \tag{B3b}$$

The partial derivative can be written as

$$\begin{aligned}
\frac{\partial V_{ij}}{\partial q_{i_k}} = \gamma^2 s\, e^s \Bigg(& T'_{i_{kxx}} \int_{-\infty}^{\infty}\int_{-\infty}^{\infty}\int_{-\infty}^{\infty} r_x^2\, e^{-s[\mathbf{T}_i : \mathbf{rr} + \mathbf{T}_j : (\mathbf{r}-\mathbf{p})(\mathbf{r}-\mathbf{p})]} dr_z\, dr_y\, dr_x + T'_{i_{kyy}} \int_{-\infty}^{\infty}\int_{-\infty}^{\infty}\int_{-\infty}^{\infty} r_y^2 \\
& \times e^{-s[\mathbf{T}_i : \mathbf{rr} + \mathbf{T}_j : (\mathbf{r}-\mathbf{p})(\mathbf{r}-\mathbf{p})]} dr_z\, dr_y\, dr_x + T'_{i_{kzz}} \int_{-\infty}^{\infty}\int_{-\infty}^{\infty}\int_{-\infty}^{\infty} r_z^2\, e^{-s[\mathbf{T}_i : \mathbf{rr} + \mathbf{T}_j : (\mathbf{r}-\mathbf{p})(\mathbf{r}-\mathbf{p})]} dr_z\, dr_y\, dr_x \\
& + 2T'_{i_{kxy}} \int_{-\infty}^{\infty}\int_{-\infty}^{\infty}\int_{-\infty}^{\infty} r_x r_y\, e^{-s[\mathbf{T}_i : \mathbf{rr} + \mathbf{T}_j : (\mathbf{r}-\mathbf{p})(\mathbf{r}-\mathbf{p})]} dr_z\, dr_y\, dr_x + 2T'_{i_{kxz}} \int_{-\infty}^{\infty}\int_{-\infty}^{\infty}\int_{-\infty}^{\infty} r_x r_z \\
& \times e^{-s[\mathbf{T}_i : \mathbf{rr} + \mathbf{T}_j : (\mathbf{r}-\mathbf{p})(\mathbf{r}-\mathbf{p})]} dr_z\, dr_y\, dr_x + 2T'_{i_{kyz}} \int_{-\infty}^{\infty}\int_{-\infty}^{\infty}\int_{-\infty}^{\infty} r_y r_z\, e^{-s[\mathbf{T}_i : \mathbf{rr} + \mathbf{T}_j : (\mathbf{r}-\mathbf{p})(\mathbf{r}-\mathbf{p})]} dr_z\, dr_y\, dr_x \Bigg).
\end{aligned} \tag{B4}$$

The required integrations are laborious but straightforward. It is useful to choose the integration order such as to simplify the final expressions obtained.

For the integrals involving r_x^2 and $r_x r_y$ the most convenient order of integration is $dr_z\, dr_y\, dr_x$ (i.e., dr_z followed by dr_y by dr_x). This yields

$$\int_{-\infty}^{\infty}\int_{-\infty}^{\infty}\int_{-\infty}^{\infty} r_x^2\, e^{-(ar_z^2 + br_z + c)} dr_z\, dr_y\, dr_x = \frac{\pi^{3/2}}{\sqrt{aa'a''}} \frac{1}{a''}\left(\frac{1}{2} + \frac{b''^2}{4a''}\right) e^{b''^2/4a'' - c''}, \tag{B5}$$

$$2\int_{-\infty}^{\infty}\int_{-\infty}^{\infty}\int_{-\infty}^{\infty} r_x r_y\, e^{-(ar_z^2 + br_z + c)}\, dr_z\, dr_y\, dr_x = \frac{\pi^{3/2}}{\sqrt{aa'a''}}\left[\frac{b'_{(1)}b''}{2a'a''} - \frac{b'_{(r_x)}}{a'a''}\left(\frac{1}{2} + \frac{b''^2}{4a''}\right)\right] e^{b''^2/4a'' - c''}, \tag{B6}$$

where a, b, c, a', a'', b', and b'' are as defined in Appendix A.

For the integrals with r_y^2 and $r_y r_z$, the most convenient order is $dr_x\, dr_z\, dr_y$. This gives expressions of the form of Eqs. (B7) and (B8) but with the parameters

$$\frac{a}{s} = T_{i_{xx}} + T_{j_{xx}}, \tag{B7a}$$

$$\frac{a'}{s} = \frac{S_{zz}S_{xx} - S_{xz}^2}{S_{xx}}, \tag{B7b}$$

$$\frac{a''}{s} = \frac{|\mathbf{T}_i + \mathbf{T}_j|}{S_{zz}S_{xx} - S_{xz}^2}, \tag{B7c}$$

$$\frac{b'}{s} = \frac{b'_{(r_y)}}{s} r_y + \frac{b'_{(1)}}{s}, \tag{B7d}$$

$$\frac{b'_{(r_y)}}{s} = 2\left(S_{zy} - \frac{S_{xz}S_{xy}}{S_{xx}}\right), \tag{B7e}$$

$$\frac{b'_{(1)}}{s}=2\left[\frac{S_{xz}}{S_{xx}}\left(T_{j_{xx}}p_x+T_{j_{xy}}p_y+T_{j_{xz}}p_z\right)-\left(T_{j_{xz}}p_x+T_{j_{yz}}p_y+T_{j_{zz}}p_z\right)\right]. \tag{B7f}$$

Again, b''/s can be written as the dot product of two vectors,

$$\frac{b''}{s}=\mathbf{B}\cdot\mathbf{p}, \tag{B7g}$$

where

$$B_x=\frac{-2}{S_{xx}S_{zz}-S_{xz}^2}\begin{vmatrix} S_{xx} & S_{xy} & S_{xz} \\ T_{j_{xx}} & T_{j_{xy}} & T_{j_{xz}} \\ S_{zx} & S_{zy} & S_{zz} \end{vmatrix}, \tag{B7h}$$

$$B_y=\frac{-2}{S_{xx}S_{zz}-S_{xz}^2}\begin{vmatrix} S_{xx} & S_{xy} & S_{xz} \\ T_{j_{yx}} & T_{j_{yy}} & T_{j_{yz}} \\ S_{zx} & S_{zy} & S_{zz} \end{vmatrix}, \tag{B7i}$$

$$B_z=\frac{-2}{S_{xx}S_{zz}-S_{xz}^2}\begin{vmatrix} S_{xx} & S_{xy} & S_{xz} \\ T_{j_{zx}} & T_{j_{zy}} & T_{j_{zz}} \\ S_{zx} & S_{zy} & S_{zz} \end{vmatrix}. \tag{B7j}$$

For the integrals involving r_z^2 and $r_x r_z$, the integration order $dr_y\,dr_x\,dr_z$ yields equations analogous to Eqs. (B7) and (B8), but with

$$\frac{a}{s}=T_{i_{yy}}+T_{j_{yy}}, \tag{B8a}$$

$$\frac{a'}{s}=\frac{S_{xx}S_{yy}-S_{xy}^2}{S_{yy}}, \tag{B8b}$$

$$\frac{a''}{s}=\frac{|\mathbf{T}_i+\mathbf{T}_j|}{S_{xx}S_{yy}-S_{xy}^2}, \tag{B8c}$$

$$\frac{b'}{s}=\frac{b'_{(r_z)}}{s}r_z+\frac{b'_{(1)}}{s}, \tag{B8d}$$

$$\frac{b'_{(r_z)}}{s}=2\left(S_{xz}-\frac{S_{xy}S_{yz}}{S_{yy}}\right), \tag{B8e}$$

$$\frac{b'_{(1)}}{s}=2\left[\frac{S_{yx}}{S_{yy}}\left(T_{j_{xy}}p_x+T_{j_{yy}}p_y+T_{j_{zy}}p_z\right)-\left(T_{j_{xx}}p_x+T_{j_{yx}}p_x+T_{j_{zx}}p_z\right)\right]. \tag{B8f}$$

Also, we have

$$\frac{b''}{s}=\mathbf{B}\cdot\mathbf{p}, \tag{B8g}$$

where

$$B_x=\frac{-2}{S_{xx}S_{yy}-S_{xy}^2}\begin{vmatrix} S_{xx} & S_{xy} & S_{xz} \\ S_{yx} & S_{yy} & S_{zy} \\ T_{j_{xx}} & T_{j_{xy}} & T_{j_{xz}} \end{vmatrix}, \tag{B8h}$$

$$B_y=\frac{-2}{S_{xx}S_{yy}-S_{xy}^2}\begin{vmatrix} S_{xx} & S_{xy} & S_{xz} \\ S_{yx} & S_{yy} & S_{zy} \\ T_{j_{yx}} & T_{j_{yy}} & T_{j_{yz}} \end{vmatrix}, \tag{B8i}$$

$$B_z=\frac{-2}{S_{xx}S_{yy}-S_{xy}^2}\begin{vmatrix} S_{xx} & S_{xy} & S_{xz} \\ S_{yx} & S_{yy} & S_{zy} \\ T_{j_{zx}} & T_{j_{zy}} & T_{j_{zz}} \end{vmatrix}. \tag{B8j}$$

The torque on particle j due to i, $\boldsymbol{\tau}_{ji}^b$, is given by

$$\boldsymbol{\tau}_{ji}^b=-\tfrac{1}{2}\tilde{\mathbf{Q}}_j\boldsymbol{\nabla}_{\mathbf{Q}_j}V_{ji}. \tag{B9}$$

If we substitute $\mathbf{r}'=\mathbf{r}-\mathbf{p}$ in Eq. (A1), $\boldsymbol{\nabla}_{\mathbf{Q}_j}V_{ji}$ can be evaluated by interchanging the labels i and j and changing the signs of all components of $\mathbf{p}$ in all relevant equations.

The numerical calculations can be simplified by noting that all integrals in Eq. (B4) contain the factor

$$I(\mathbf{p},\mathbf{q}_i,\mathbf{q}_j)=\frac{\pi^{3/2}\gamma^2\,e^{b''^2/4a''-c''}}{\sqrt{aa'a''}},$$

which is independent of integration order and choice of origin. It is only necessary to calculate this term once, e.g., when the pair energy is evaluated. This means that only parts of the prefactors occurring in Eqs. (B7) and (B8) must be recalculated in order to determine all the integrals occurring in Eq. (B4). This is also true of the jth particle torques.

[1] P. S. Simmonds and G. R. Luckhurst, Mol. Phys. **80**, 233 (1993).
[2] D. Frenkel, H. N. W. Lekkerkerker, and A. Stroobants, Nature **332**, 822 (1988).
[3] D. Frenkel, Liq. Cryst. **5**, 929 (1989).
[4] D. Frenkel, B. M. Mulder, and J. P. McTague, Phys. Rev. Lett. **52**, 287 (1984); D. Frenkel and B. M. Mulder, Mol. Phys. **55**, 1171 (1985).
[5] M. P. Allen, G. T. Evans, D. Frenkel, and B. M. Mulder, Adv. Chem. Phys. **86**, 1 (1993).
[6] M. P. Allen, Liq. Cryst. **8**, 499 (1990).
[7] B. J. Berne and P. Pechukas, J. Chem. Phys. **56**, 4213 (1972).
[8] J. G. Gay and B. J. Berne, J. Chem. Phys. **74**, 3316 (1981).
[9] D. J. Adams, G. R. Luckhurst, and R. W. Phippen, Mol. Phys. **61**, 1575 (1987).
[10] E. de Miguel and L. F. Rull, Mol. Phys. **74**, 405 (1991).
[11] E. de Miguel, L. F. Rull, M. K. Chalam, and K. E. Gubbins, Mol. Phys. **74**, 405 (1991).
[12] E. de Miguel, L. F. Rull, M. K. Chalam, K. E. Gubbins, and F. van Swol, Mol. Phys. **72**, 593 (1991).
[13] G. R. Luckhurst and G. W. Gray, *The Molecular Physics of Liquid Crystals* (Academic, London, 1979), Chap. 1.
[14] M. P. Allen and D. J. Tildesely, *Computer Simulation of Liquids* (Clarendon, Oxford, 1989).
[15] J. P. Straley, Phys. Rev. A **10**, 1881 (1974).
[16] M. P. Allen, Mol. Phys. **52**, 717 (1984).
[17] G. J. Zarragoicoechea, D. Levesque, and J. J. Weis, Mol. Phys. **75**, 998 (1992).